

Pion photoproduction on the nucleon in the quark model

Qiang Zhao,^{1,*} J. S. Al-Khalili,¹ Z.-P. Li,² and R.L. Workman³

¹*Department of Physics, University of Surrey, Guildford, Surrey GU2 7XH, United Kingdom*

²*Department of Physics, Peking University, 100871 Beijing, People's Republic of China*

³*Center for Nuclear Studies and Department of Physics, The George Washington University, Washington, D.C. 20052*

(Received 18 February 2002; published 20 June 2002)

We present a detailed quark-model study of pion photoproduction within the effective Lagrangian approach. Cross sections and single-polarization observables are investigated for the four charge channels, $\gamma p \rightarrow \pi^+ n$, $\gamma n \rightarrow \pi^- p$, $\gamma p \rightarrow \pi^0 p$, and $\gamma n \rightarrow \pi^0 n$. Leaving the $\pi N \Delta$ coupling strength to be a free parameter, we obtain a reasonably consistent description of these four channels from threshold to the first resonance region. Within this effective Lagrangian approach, strongly constrained by the quark model, we consider the issue of double counting which may occur if additional t -channel contributions are included.

DOI: 10.1103/PhysRevC.65.065204

PACS number(s): 12.39.-x, 13.60.Le, 14.20.Gk, 25.20.Lj

I. INTRODUCTION

Pion photoproduction has provided a wealth of information about baryon resonances. During the past three or four decades, extensive investigations have been carried out in both experiment and theory. In particular, the recent availability of high intensity electron and photon beams at JLab, ELSA, MAMI, and ESRF has significantly improved the precision of pion photo- and electroproduction experiments. A large experimental database now exists, and a significant increase is expected once the current set of experiments has been analyzed.

Pion photoproduction has been an important source, supplementary to πN scattering experiments, for establishing most of the well-known baryon resonances, while providing information on their photodecay amplitudes. In the search for “missing resonances,” other meson production channels, to which these resonances might have stronger couplings, are now being extensively studied (see, e.g., Ref. [1], and references therein).

Apart from a few dominant states, a considerable model dependence exists in resonance parameters extracted using phenomenological approaches to the data. This has complicated the comparison with resonance parameters derived from quark models. Historically, most approaches have adopted a factorization of the meson interaction vertices, where the dynamical information is absorbed into the resonance partial-decay widths and empirical form factors. Consequently, parameters for the meson-nucleon-resonance couplings and form factors have been introduced.

Such empirical schemes have been very important in analyses of data and the extraction of resonance signals in pion photoproduction [2]. A number of multipole fits, taking into account different dynamical aspects, are now underway. For instance, the unitary isobar model (MAID) [3], containing Born terms, five resonances, and vector-meson exchanges, succeeds in the description of data up to 1 GeV. Approaches adopting constraints from fixed- t dispersion relations are being revisited and applied to the delta region [4–6]. Other

approaches, using effective Lagrangians for the Delta resonance excitation and t -channel vector-meson exchange, can also be found in the literature [7–11]. The SAID fits [12,13], based on a parametrization of different partial wave contributions, extend the analysis up to 2 GeV. With some common features but quite different model constraints, these multipole fits hope to converge to a common result and obtain, as near as possible, model-independent information on the resonance excitations.

There is a clear need to treat all resonances consistently, and to understand the relation between the s - and u -channel resonances and t -channel meson exchanges. A recently developed quark-model framework [14], augmented by an effective Lagrangian approach to reaction dynamics, provides a good starting point. The main feature of this model is the introduction of an effective chiral Lagrangian for the quark-pseudoscalar-meson coupling in a constituent quark model. Unlike most previous quark models, which were generally based on factorization of the strong interaction vertices, the pion is treated as an elementary particle. As a result, one can explicitly calculate the tree level diagrams for pion production reactions. Here, the quark-model wave functions for the nucleons and baryon resonances provide a form factor for each interaction vertex, and all the s - and u -channel resonances can be consistently included.

This model has the advantage of being able to describe a large photoproduction database, employing only a very limited number of parameters within a microscopic framework. Applications of this model to the η [15–18] and K [19,20] meson photoproduction have been quite successful, and this has motivated our study of the very extensive pion photoproduction database.

The quark model's well-known underestimation of the electromagnetic (EM) transition amplitude for the delta resonance makes this resonance region particularly interesting. As suggested in Ref. [11], the “bare” $\gamma N \rightarrow \Delta$ vertex could be more directly related to the quantity given by the quark-model derivation of the delta EM transition. A direct examination of the delta excitation in $\gamma N \rightarrow \Delta \rightarrow \pi N$ might shed some light on this question.

This paper presents both quantitative and qualitative investigations of pion photoproduction. The challenge to de-

*Email address: qiang.zhao@surrey.ac.uk

scribe the N^* resonance excitation with explicit quark and gluon degrees of freedom is by no means trivial, since the correct off-shell behavior of those intermediate resonances is required. Also, a clear definition of the nucleon Born terms, associated with the gauge invariance requirement, is essential for this effective theory. In this study, we concentrate on the energy region corresponding to $E_\gamma \lesssim 700$ MeV, where the role played by the Born terms¹ and the low-lying resonances, in particular the $\Delta(1232)$, $S_{11}(1535)$, and $D_{13}(1520)$, can be clarified. Qualitative tests have been made in order to compare this model to a typical isobaric approach. Here we consider the role played by the t -channel vector meson exchanges in isobaric models, and the effect of neglecting the u -channel resonance contributions.

In Sec. II, we outline the formalism aspects of our approach. In Sec. III, results for cross sections and single-polarization asymmetries for the four charge channels, $\gamma p \rightarrow \pi^+ n$, $\gamma p \rightarrow \pi^0 p$, $\gamma n \rightarrow \pi^- p$, and $\gamma n \rightarrow \pi^0 n$ will be presented. The role of the t -channel vector-meson exchange will also be discussed. Conclusions are drawn in Sec. IV.

II. THE MODEL

Before we begin a detailed analysis, a brief review of this model is necessary.

A. The effective Lagrangian

For pion photoproduction, the low-energy theorem (LET) provides a crucial test near threshold. As shown in previous investigation by Li [21], to recover the LET, one has to rely on the low-energy QCD Lagrangian which keeps the meson-baryon interaction invariant under the chiral transformation. Combining the low-energy QCD Lagrangian with the quark model, we introduce the quark-meson interaction through the effective Lagrangian [14]:

$$\mathcal{L} = \bar{\psi} [\gamma_\mu (i \partial^\mu + V^\mu + \gamma_5 A^\mu) - m] \psi + \dots, \quad (1)$$

where the vector and axial currents are

$$V_\mu = \frac{1}{2} (\xi^\dagger \partial_\mu \xi + \xi \partial_\mu \xi^\dagger),$$

$$A_\mu = i \frac{1}{2} (\xi^\dagger \partial_\mu \xi - \xi \partial_\mu \xi^\dagger), \quad (2)$$

and the chiral transformation is

$$\xi = e^{i \phi_m / f_m}, \quad (3)$$

where f_m is the decay constant of the meson. The quark field ψ in the SU(3) symmetry is

$$\psi = \begin{pmatrix} \psi(u) \\ \psi(d) \\ \psi(s) \end{pmatrix}, \quad (4)$$

and the meson field ϕ_m is a $3 \otimes 3$ matrix:

$$\phi_m = \begin{pmatrix} \frac{1}{\sqrt{2}} \pi^0 + \frac{1}{\sqrt{6}} \eta & \pi^+ & K^+ \\ \pi^- & -\frac{1}{\sqrt{2}} \pi^0 + \frac{1}{\sqrt{6}} \eta & K^0 \\ K^- & \bar{K}^0 & -\sqrt{\frac{2}{3}} \eta \end{pmatrix}, \quad (5)$$

where the pseudoscalar mesons π , η , and K are treated as Goldstone bosons. Thus, the Lagrangian in Eq. (1) is invariant under the chiral transformation. Expanding the nonlinear field ξ in Eq. (3) in terms of the Goldstone boson field ϕ_m , i.e., $\xi = 1 + i \phi_m / f_m + \dots$, we obtain the standard quark-meson pseudovector coupling at tree level:

$$H_m = \sum_j \frac{1}{f_m} \bar{\psi}_j \gamma_\mu^j \gamma_5^j \psi_j \partial^\mu \phi_m, \quad (6)$$

where ψ_j ($\bar{\psi}_j$) represents the j th quark (antiquark) field in the nucleon.

It is still not clear whether the Goldstone bosons couple to the nucleon through a pseudoscalar or pseudovector coupling, or even both. To our present knowledge, at low energies, the pseudovector coupling satisfies partial conservation of axial current and is consistent with the LET and chiral perturbation theory to leading order, while the high-energy study prefers a pseudoscalar coupling. As pointed out in Ref. [22], the operators for the pseudoscalar and pseudovector coupling have the same leading order expression at quark tree level. Therefore, Eq. (6) can be regarded as a reasonable starting point for investigations of pion photoproduction in the resonance region.

The quark-photon electromagnetic coupling is

$$H_e = - \sum_j e_j \gamma_\mu^j A^\mu(\mathbf{k}, \mathbf{r}), \quad (7)$$

where the photon has three momentum \mathbf{k} , and the constituent quark carries a charge e_j .

The photoproduction amplitudes can be expressed in terms of the Mandelstam variables,

$$M_{fi} = M_{fi}^{sg} + M_{fi}^s + M_{fi}^u + M_{fi}^t, \quad (8)$$

where M_{fi}^{sg} is the seagull term and M_{fi}^s , M_{fi}^u , and M_{fi}^t represent the s -, u -, and t -channel processes as illustrated in Fig. 1. As shown in Ref. [14], the seagull term is composed of two parts,

$$M_{fi}^{sg} = \langle N_f | H_{m,e} | N_i \rangle + i \langle N_f | [g_e, H_m] | N_i \rangle, \quad (9)$$

¹We use ‘‘Born terms’’ here to denote the amplitudes from a Born approximation, in which the nucleon pole terms, pion pole, and contact term are included. In the following sections, we use ‘‘nucleon pole terms’’ to denote the s - and u -channel nucleon exchange amplitudes.

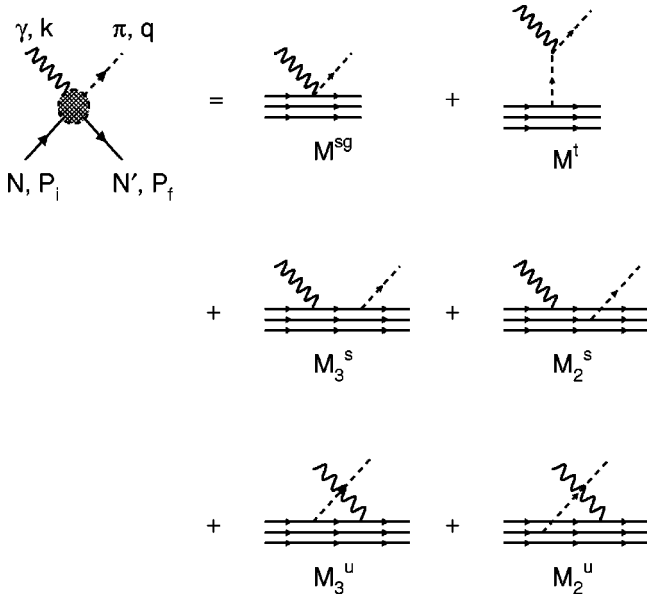


FIG. 1. Tree level diagrams calculated in this model.

where $|N_i\rangle$ and $|N_f\rangle$ are the initial and final state nucleons, respectively,

$$H_{m,e} = \sum_j \frac{e_m}{f_m} \phi_m(\mathbf{q}, \mathbf{r}_j) \bar{\psi}_j \gamma_\mu^j \gamma_5^j \psi_j A^\mu(\mathbf{k}, \mathbf{r}_j) \quad (10)$$

is the contact term from the pseudovector coupling, and

$$g_e = \sum_j e_j \mathbf{r}_j \cdot \boldsymbol{\epsilon}_\gamma e^{i\mathbf{k} \cdot \mathbf{r}_j} \quad (11)$$

comes from the transformation of the electromagnetic interaction in the s and u channels [23,14].

The s - and u -channel amplitudes have the following expression:

$$\begin{aligned} M_{fi}^s + M_{fi}^u &= i\omega_\gamma \sum_j \langle N_f | H_m | N_j \rangle \langle N_j | \frac{1}{E_i + \omega_\gamma - E_j} h_e | N_i \rangle \\ &+ i\omega_\gamma \sum_j \langle N_f | h_e \frac{1}{E_i - \omega_m - E_j} | N_j \rangle \langle N_j | H_m | N_i \rangle, \end{aligned} \quad (12)$$

where

$$h_e = \sum_j e_j \mathbf{r}_j \cdot \boldsymbol{\epsilon}_\gamma (1 - \boldsymbol{\alpha}_j \cdot \hat{\mathbf{k}}) e^{i\mathbf{k} \cdot \mathbf{r}_j}, \quad (13)$$

and $\hat{\mathbf{k}} \equiv \mathbf{k}/\omega_\gamma$ is the unit vector in the direction of the photon momentum.

The nonrelativistic expansions of Eqs. (13) and (6) become [14]

$$h_e = \sum_j \left[e_j \mathbf{r}_j \cdot \boldsymbol{\epsilon}_\gamma - \frac{e_j}{2m_j} \boldsymbol{\sigma}_j \cdot (\boldsymbol{\epsilon}_\gamma \times \hat{\mathbf{k}}) \right] e^{i\mathbf{k} \cdot \mathbf{r}_j}, \quad (14)$$

and

$$\begin{aligned} H_m^{nr} &= \sum_j \left[\frac{\omega_m}{E_f + M_f} \boldsymbol{\sigma}_j \cdot \mathbf{P}_f + \frac{\omega_m}{E_i + M_i} \boldsymbol{\sigma}_j \cdot \mathbf{P}_i \right. \\ &\quad \left. - \boldsymbol{\sigma}_j \cdot \mathbf{q} + \frac{\omega_m}{2\mu_q} \boldsymbol{\sigma}_j \cdot \mathbf{p}_j \right] \frac{\hat{I}_j}{g_A} e^{-i\mathbf{q} \cdot \mathbf{r}_j}, \end{aligned} \quad (15)$$

where M_i (M_f), E_i (E_f), and \mathbf{P}_i (\mathbf{P}_f) are mass, energy, and three-vector momentum for the initial (final) nucleon; \mathbf{r}_j and \mathbf{p}_j are the internal coordinate and momentum for the j th quark in the nucleon rest system. Note that g_A , the axial vector coupling, relates the hadronic operator $\boldsymbol{\sigma}$ to the quark operator $\boldsymbol{\sigma}_j$ for the j th quark, and is defined by

$$\langle N_f | \sum_j \hat{I}_j \boldsymbol{\sigma}_j | N_i \rangle \equiv g_A \langle N_f | \boldsymbol{\sigma} | N_i \rangle. \quad (16)$$

The transition amplitudes of pseudoscalar-meson photoproduction can generally be expressed in terms of standard Chew-Goldberger-Low-Nambu (CGLN) amplitudes [24], i.e.,

$$M_{fi} = \mathbf{J} \cdot \boldsymbol{\epsilon}_\gamma, \quad (17)$$

where \mathbf{J} is the interaction current and can be related to the CGLN amplitudes $f_{1,2,3,4}$:

$$\begin{aligned} \mathbf{J} &= f_1 \boldsymbol{\sigma} + i f_2 \frac{(\boldsymbol{\sigma} \cdot \mathbf{q})(\mathbf{k} \times \boldsymbol{\sigma})}{|\mathbf{q}||\mathbf{k}|} \\ &+ f_3 \frac{\boldsymbol{\sigma} \cdot \mathbf{k}}{|\mathbf{q}||\mathbf{k}|} \mathbf{q} + f_4 \frac{\boldsymbol{\sigma} \cdot \mathbf{q}}{\mathbf{q}^2} \mathbf{q}. \end{aligned} \quad (18)$$

Alternatively, one can express the transition amplitudes in the helicity space in terms of the \mathcal{T} matrix:

$$H_1 = \langle \lambda_f = +1/2 | \mathcal{T} | \lambda_\gamma = +1, \lambda_i = -1/2 \rangle,$$

$$H_2 = \langle \lambda_f = +1/2 | \mathcal{T} | \lambda_\gamma = +1, \lambda_i = +1/2 \rangle,$$

$$H_3 = \langle \lambda_f = -1/2 | \mathcal{T} | \lambda_\gamma = +1, \lambda_i = -1/2 \rangle,$$

$$H_4 = \langle \lambda_f = -1/2 | \mathcal{T} | \lambda_\gamma = +1, \lambda_i = +1/2 \rangle, \quad (19)$$

where λ_i and λ_f are helicities of the initial and final nucleons and λ_γ is the helicity of the photon. Amplitudes with

$\lambda_\gamma = -1$ are not independent of those with $\lambda_\gamma = +1$ due to parity conservation. The CGLN and helicity amplitudes may be related through a standard transformation [25].

B. Transition amplitudes in the harmonic oscillator basis

The seagull term in this model differs from the traditional definition due to the appearance of a transformed electromagnetic interaction coupling to the meson at the same vertex. This term can be worked out explicitly in the $SU(6) \otimes O(3)$ symmetry limit:

$$M_{fi}^{sg} = -e^{-(\mathbf{k}-\mathbf{q})^2/6\alpha^2} e_m \times \left[1 + \frac{\omega_m}{2} \left(\frac{1}{E_i + M_i} + \frac{1}{E_f + M_f} \right) \right] \boldsymbol{\sigma} \cdot \boldsymbol{\epsilon}_\gamma, \quad (20)$$

where the exponential factor is the corresponding quark-model form factor in the harmonic oscillator basis.

The t -channel charged pion exchange amplitude can be derived by treating the exchanged pion as an elementary particle:

$$M_{fi}^t = e^{-(\mathbf{k}-\mathbf{q})^2/6\alpha^2} \frac{e_m(M_f + M_i)}{q \cdot k} \times \left(\frac{\boldsymbol{\sigma} \cdot \mathbf{q}}{E_f + M_f} - \frac{\boldsymbol{\sigma} \cdot \mathbf{k}}{E_i + M_i} \right) \mathbf{q} \cdot \boldsymbol{\epsilon}_\gamma, \quad (21)$$

where q and k are four-vector momenta of the pion and photon, respectively.

As illustrated in Eqs. (20) and (21), the leading order amplitudes from chiral perturbation theory are reproduced. The quark-model modifications to these two terms come from three-body effects, which add an additional term [the second term in Eq. (20)] to the amplitudes. Note also the appearance of a form factor, which is essential to sustain the forward ‘‘spike’’ in π^+ production.

Generalized expressions for the s - and u -channel amplitudes are

and

$$M_{fi}^s = \sum_n (M_2^s + M_3^s) e^{-(\mathbf{k}^2 + \mathbf{q}^2)/6\alpha^2}, \quad (22)$$

$$M_{fi}^u = \sum_n (M_2^u + M_3^u) e^{-(\mathbf{k}^2 + \mathbf{q}^2)/6\alpha^2}, \quad (23)$$

where the M_3 and M_2 represent transitions in which the photon and meson couple to the same quark or different quarks, respectively. The general framework was presented in Ref. [14]. Here, we present the transition amplitudes in terms of the harmonic oscillator shell n as follows:

$$\begin{aligned} \frac{M_3^s}{g_3^s} = & -\frac{1}{2m_q} [ig_v \mathbf{A}_s \cdot (\boldsymbol{\epsilon}_\gamma \times \mathbf{k}) - \boldsymbol{\sigma} \cdot \{\mathbf{A}_s \times (\boldsymbol{\epsilon}_\gamma \times \mathbf{k})\}] \\ & \times \frac{M_n}{n!(P_i \cdot k - nM\omega_h)} \left(\frac{\mathbf{k} \cdot \mathbf{q}}{3\alpha^2} \right)^n \\ & + \frac{1}{6} \left[\frac{\omega_\gamma \omega_m}{\mu_q} \left(1 + \frac{\omega_\gamma}{2m_q} \right) \boldsymbol{\sigma} \cdot \boldsymbol{\epsilon}_\gamma + \frac{2\omega_\gamma}{\alpha^2} \boldsymbol{\sigma} \cdot \mathbf{A}_s \boldsymbol{\epsilon}_\gamma \cdot \mathbf{q} \right] \\ & \times \frac{M_n}{(n-1)!(P_i \cdot k - nM\omega_h)} \left(\frac{\mathbf{k} \cdot \mathbf{q}}{3\alpha^2} \right)^{n-1} \\ & + \frac{\omega_\gamma \omega_m}{18\mu_q \alpha^2} \boldsymbol{\sigma} \cdot \mathbf{k} \boldsymbol{\epsilon}_\gamma \cdot \mathbf{q} \\ & \times \frac{M_n}{(n-2)!(P_i \cdot k - nM\omega_h)} \left(\frac{\mathbf{k} \cdot \mathbf{q}}{3\alpha^2} \right)^{n-2} \end{aligned} \quad (24)$$

and

$$\begin{aligned} \frac{M_2^s(-2)^n}{g_2^s} = & -\frac{1}{2m_q} [ig'_v \mathbf{A}_s \cdot (\boldsymbol{\epsilon}_\gamma \times \mathbf{k}) - g'_a \boldsymbol{\sigma} \cdot \{\mathbf{A}_s \times (\boldsymbol{\epsilon}_\gamma \times \mathbf{k})\}] \frac{M_n}{n!(P_i \cdot k - nM\omega_h)} \left(\frac{\mathbf{k} \cdot \mathbf{q}}{3\alpha^2} \right)^n + \frac{1}{6} \left[\frac{\omega_\gamma \omega_m}{\mu_q} \left(1 + g'_a \frac{\omega_\gamma}{2m_q} \right) \boldsymbol{\sigma} \cdot \boldsymbol{\epsilon}_\gamma \right. \\ & \left. + \frac{2\omega_\gamma}{\alpha^2} \boldsymbol{\sigma} \cdot \mathbf{A}_s \boldsymbol{\epsilon}_\gamma \cdot \mathbf{q} \right] \frac{M_n}{(n-1)!(P_i \cdot k - nM\omega_h)} \left(\frac{\mathbf{k} \cdot \mathbf{q}}{3\alpha^2} \right)^{n-1} + \frac{\omega_\gamma \omega_m}{18\mu_q \alpha^2} \boldsymbol{\sigma} \cdot \mathbf{k} \boldsymbol{\epsilon}_\gamma \cdot \mathbf{q} \frac{M_n}{(n-2)!(P_i \cdot k - nM\omega_h)} \left(\frac{\mathbf{k} \cdot \mathbf{q}}{3\alpha^2} \right)^{n-2} \end{aligned} \quad (25)$$

are results for the s channel, while

$$\begin{aligned}
 \frac{M_3^u}{g_3^u} &= \frac{1}{2m_q} [ig_v \mathbf{A}_u \cdot (\boldsymbol{\epsilon}_\gamma \times \mathbf{k}) + \boldsymbol{\sigma} \cdot \{\mathbf{A}_u \times (\boldsymbol{\epsilon}_\gamma \times \mathbf{k})\}] \\
 &\times \frac{M_n}{n!(P_f \cdot k + nM\omega_h)} \left(\frac{\mathbf{k} \cdot \mathbf{q}}{3\alpha^2} \right)^n \\
 &- \frac{1}{6} \left[\frac{\omega_\gamma \omega_m}{\mu_q} \left(1 + \frac{\omega_\gamma}{2m_q} \right) \boldsymbol{\sigma} \cdot \boldsymbol{\epsilon}_\gamma + \frac{2\omega_\gamma}{\alpha^2} \boldsymbol{\sigma} \cdot \mathbf{A}_u \boldsymbol{\epsilon}_\gamma \cdot \mathbf{q} \right] \\
 &\times \frac{M_n}{(n-1)!(P_f \cdot k + nM\omega_h)} \left(\frac{\mathbf{k} \cdot \mathbf{q}}{3\alpha^2} \right)^{n-1} \\
 &- \frac{\omega_\gamma \omega_m}{18\mu_q \alpha^2} \boldsymbol{\sigma} \cdot \mathbf{k} \boldsymbol{\epsilon}_\gamma \cdot \mathbf{q} \\
 &\times \frac{M_n}{(n-2)!(P_f \cdot k + nM\omega_h)} \left(\frac{\mathbf{k} \cdot \mathbf{q}}{3\alpha^2} \right)^{n-2} \quad (26)
 \end{aligned}$$

and

$$\begin{aligned}
 \frac{M_2^u(-2)^n}{g_2^u} &= \frac{1}{2m_q} [ig'_v \mathbf{A}_u \cdot (\boldsymbol{\epsilon}_\gamma \times \mathbf{k}) \\
 &- g'_a \boldsymbol{\sigma} \cdot \{\mathbf{A}_u \times (\boldsymbol{\epsilon}_\gamma \times \mathbf{k})\}] \frac{M_n}{n!(P_f \cdot k + nM\omega_h)} \\
 &\times \left(\frac{\mathbf{k} \cdot \mathbf{q}}{3\alpha^2} \right)^n - \frac{1}{6} \left[\frac{\omega_\gamma \omega_m}{\mu_q} \left(1 + g'_a \frac{\omega_\gamma}{2m_q} \right) \boldsymbol{\sigma} \cdot \boldsymbol{\epsilon}_\gamma \right. \\
 &\left. + \frac{2\omega_\gamma}{\alpha^2} \boldsymbol{\sigma} \cdot \mathbf{A}_u \boldsymbol{\epsilon}_\gamma \cdot \mathbf{q} \right] \frac{M_n}{(n-1)!(P_f \cdot k + nM\omega_h)} \\
 &\times \left(\frac{\mathbf{k} \cdot \mathbf{q}}{3\alpha^2} \right)^{n-1} - \frac{\omega_\gamma \omega_m}{18\mu_q \alpha^2} \boldsymbol{\sigma} \cdot \mathbf{k} \boldsymbol{\epsilon}_\gamma \cdot \mathbf{q} \\
 &\times \frac{M_n}{(n-2)!(P_f \cdot k + nM\omega_h)} \left(\frac{\mathbf{k} \cdot \mathbf{q}}{3\alpha^2} \right)^{n-2} \quad (27)
 \end{aligned}$$

are corresponding terms for the u channel. Vectors \mathbf{A}_s and \mathbf{A}_u are determined by the meson transitions in the s and u channels:

$$\mathbf{A}_s = - \left(\frac{\omega_m}{E_f + M_f} + 1 \right) \mathbf{q} \quad (28)$$

and

$$\begin{aligned}
 \mathbf{A}_u &= - \left(\frac{\omega_m}{E_i + M_i} + \frac{\omega_m}{E_f + M_f} \right) \mathbf{k} \\
 &- \left(\frac{\omega_m}{E_f + M_f} + 1 \right) \mathbf{q}. \quad (29)
 \end{aligned}$$

In Eqs. (24)–(27), P_i and P_f are four-vector momenta of the initial and final state nucleons in the total c.m. system; M_n is the mass of the excited state in the n th shell, while $\omega_h (= \alpha^2/m_q)$ is the typical energy of the harmonic oscillator potential. The factors $M_n/(P_i \cdot k - nM\omega_h)$ and $M_n/(P_f \cdot k + nM\omega_h)$ have clear physical meanings in the s and u channels that can be related to the propagators.

The quark level operators have been related to the hadronic level ones through g factors defined as below:

$$g_3^u = \langle N_f | \sum_j e_j \hat{I}_j \sigma_j^z | N_i \rangle / g_A, \quad (30)$$

$$g_2^u = \langle N_f | \sum_{i \neq j} e_j \hat{I}_i \sigma_i^z | N_i \rangle / g_A, \quad (31)$$

$$g_v = \frac{1}{g_3^u g_A} \langle N_f | \sum_j e_j \hat{I}_j | N_i \rangle, \quad (32)$$

$$g'_v = \frac{1}{3g_2^u g_A} \langle N_f | \sum_{i \neq j} e_j \hat{I}_i \sigma_i \cdot \sigma_j | N_i \rangle, \quad (33)$$

and

$$g'_a = \frac{1}{2g_2^u g_A} \langle N_f | \sum_{i \neq j} e_j \hat{I}_i (\boldsymbol{\sigma}_i \times \boldsymbol{\sigma}_j)_z | N_i \rangle. \quad (34)$$

Numerical values for these g factors can be explicitly calculated in the $SU(6) \otimes O(3)$ symmetry limit [14].

So far, the resonance contributions have not been explicitly separated out. The intermediate states are still degenerate in the quantum number of the harmonic oscillator shell. Notice that the factor $M_n/(P_i \cdot k - nM\omega_h)$ can be written as $2M_n/(s - M_n^2)$, where $s = W^2 = (P_i + k)^2$ is the square of the total c.m. energy. We thus substitute a Breit-Wigner distribution for the resonances, $2M_R/[s - M_R^2 + iM_R\Gamma_R(\mathbf{q})]$, where the resonance mass and width effects are taken into account. Explicitly, all the contributing resonances with $n \leq 2$ in the quark-model symmetry limit can be included. In pion production, this is the place where the imaginary part of the transition amplitude comes out. The role of the imaginary part can be investigated more directly in the polarization observables, e.g., polarized target asymmetry T and recoil polarization asymmetry P , where direct interferences between the real and imaginary parts are highlighted.

Consequently, we must separate out the resonance excitation amplitudes for each n . For $n=0$, the contributing terms are the delta resonance excitation and the nucleon pole terms. One can see that only the first terms in Eqs. (24)–(27) can contribute. For the s channel, we have

$$\begin{aligned}
M^s(n=0) = & -\frac{1}{2m_q} [i(g_3^s g_v + g_2^u g_v') \mathbf{A}_s \cdot (\boldsymbol{\epsilon}_\gamma \times \mathbf{k}) \\
& - (g_3^s + g_2^u g_a') \boldsymbol{\sigma} \cdot \{\mathbf{A}_s \times (\boldsymbol{\epsilon}_\gamma \times \mathbf{k})\}] \\
& \times \frac{M_0}{P_i \cdot k - \delta M^2/2} e^{-(\mathbf{k}^2 + \mathbf{q}^2)/6\alpha^2}, \quad (35)
\end{aligned}$$

where $\delta M^2/2$ denotes the mass square difference between the intermediate state and initial state nucleon. The amplitude for the spin 1/2 nucleon pole term is

$$\begin{aligned}
M^s(\text{nucleon}) = & \langle N_f | H_m | N(J=1/2) \rangle \langle N(J=1/2) | h_e | N_i \rangle \\
= & -\frac{i\mu_i}{2m_q} \boldsymbol{\sigma} \cdot \mathbf{A}_s \boldsymbol{\sigma} \cdot (\boldsymbol{\epsilon}_\gamma \times \mathbf{k}) \frac{2M_N}{s - M_N^2} e^{-(\mathbf{k}^2 + \mathbf{q}^2)/6\alpha^2}, \quad (36)
\end{aligned}$$

where we have used $\delta M^2/2=0$ and $P_i \cdot k = (s - M_N^2)/2$ for the nucleon pole; μ_i is the magnetic moment of the initial nucleon in terms of the proton magnetic moment $e/2m_q$. In this way, the delta resonance excitation amplitude is derived,

$$\begin{aligned}
M^s(\Delta) = & M^s(n=0) - M^s(\text{nucleon}) \\
= & -\frac{1}{2m_q} [i(g_3^s g_v + g_2^u g_v' - \mu_i) \mathbf{A}_s \cdot (\boldsymbol{\epsilon}_\gamma \times \mathbf{k}) \\
& - (g_3^s + g_2^u g_a' - \mu_i) \boldsymbol{\sigma} \cdot \{\mathbf{A}_s \times (\boldsymbol{\epsilon}_\gamma \times \mathbf{k})\}] \\
& \times \frac{2M_\Delta}{s - M_\Delta^2 + iM_\Delta \Gamma_\Delta} e^{-(\mathbf{k}^2 + \mathbf{q}^2)/6\alpha^2}, \quad (37)
\end{aligned}$$

where $M_0/(P_i \cdot k - \delta M^2/2) \equiv M_\Delta/[s - M_N^2 - (M_\Delta^2 - M_N^2)]/2$ is used and the Breit-Wigner distribution is introduced after the separation of the spin operators.

Similarly, the delta resonance and nucleon pole terms in the u channel with $n=0$ can be separated:

$$\begin{aligned}
M^u(\text{nucleon}) = & \langle N_f | h_e | N(J=1/2) \rangle \langle N(J=1/2) | H_m | N_i \rangle \\
= & -\frac{i\mu_f}{2m_q} \boldsymbol{\sigma} \cdot (\boldsymbol{\epsilon}_\gamma \times \mathbf{k}) \boldsymbol{\sigma} \cdot \mathbf{A}_u \\
& \times \frac{2M_N}{u - M_N^2} e^{-(\mathbf{k}^2 + \mathbf{q}^2)/6\alpha^2}, \quad (38)
\end{aligned}$$

and

$$\begin{aligned}
M^u(\Delta) = & -\frac{1}{2m_q} [i(g_3^u g_v + g_2^u g_v' - \mu_f) \mathbf{A}_u \cdot (\boldsymbol{\epsilon}_\gamma \times \mathbf{k}) \\
& + (g_3^u - g_2^u g_a' - \mu_f) \boldsymbol{\sigma} \cdot \{\mathbf{A}_u \times (\boldsymbol{\epsilon}_\gamma \times \mathbf{k})\}] \\
& \times \frac{2M_\Delta}{u - M_\Delta^2} e^{-(\mathbf{k}^2 + \mathbf{q}^2)/6\alpha^2}, \quad (39)
\end{aligned}$$

where μ_f is the magnetic moment of the final state nucleon in terms of the proton magnetic moment $e/2m_q$.

Several points can be learned from Eqs. (24)–(27). First, the nucleon pole terms and delta resonance transition only involve the c.m. part of their spatial wave functions. Therefore, only the first terms in these equations contribute to the amplitudes. For resonances with $n>0$, the internal motion of constituents will be involved. Specifically, terms relating to $(n-1)$ are due to correlations between c.m. motion and internal ones, while $(n-2)$ terms are due to correlations between internal motions at two vertices.

Secondly, amplitudes for processes having the photon and meson coupled to different quarks are relatively suppressed. This can be seen clearly through the factors $(-2)^n$. In Ref. [26], this qualitative feature was discussed, but not shown explicitly. Here, we show how the indirect diagram can be exactly calculated, and show that the direct diagram will become dominant with increasing energy and the excitation of higher states.

Notice that in the degeneracy limit, the sum over n in Eqs. (24)–(27), gives

$$\begin{aligned}
M_{fi}^s + M_{fi}^u = & \sum_{n=0}^{\infty} (\hat{O}_s + \hat{O}_u) \frac{1}{n!} \left(\frac{\mathbf{k} \cdot \mathbf{q}}{3\alpha^2} \right)^n e^{-(\mathbf{k}^2 + \mathbf{q}^2)/6\alpha^2} \\
= & (\hat{O}_s + \hat{O}_u) e^{-(\mathbf{k} - \mathbf{q})^2/6\alpha^2}, \quad (40)
\end{aligned}$$

where \hat{O}_s and \hat{O}_u represent operators independent of n , and recovering the factor $e^{-(\mathbf{k} - \mathbf{q})^2/6\alpha^2}$ is essential for the theory to be gauge invariant. Although like many other phenomenological approaches this model does not have unitarity, such a form factor prevents certain terms from violating unitarity. One can see that at high energies the degeneracy limit can be recognized by the dominance of the direct diagram. How to restore the unitarity in a general framework should be a next step of this investigation.

From Eq. (37), the analytical expression for the delta multipole can be derived,

$$\begin{aligned}
M_{1+}^{3/2} = & -g_{\pi NN} g_R \frac{1}{2m_q} \left[\frac{\omega_m}{E_f + M_f} + 1 \right] \\
& \times \frac{2M_\Delta}{s - M_\Delta^2 + iM_\Delta \Gamma_\Delta} e^{-(\mathbf{k}^2 + \mathbf{q}^2)/6\alpha^2}, \quad (41)
\end{aligned}$$

where $g_R \equiv g_3^s g_v + g_2^u g_v' - \mu_i$, and $g_{\pi NN}$ has been taken into account. The real and imaginary parts of the delta multipole $M_{1+}^{3/2}$ are calculated and shown in Fig. 2. We shall discuss the quark-model form factor effects in the following section. Therefore, it would be useful to present the calculation of $M_{1+}^{3/2}$ without the exponent, which comes from the spatial integral and serves as a form factor for the multipole. As illustrated by the dotted and dot-dashed curves in Fig. 2, apparent deviations from the experimental data occur with the increasing energies. In other words, the quark model turns out to be indispensable to account for the correct energy dependence.

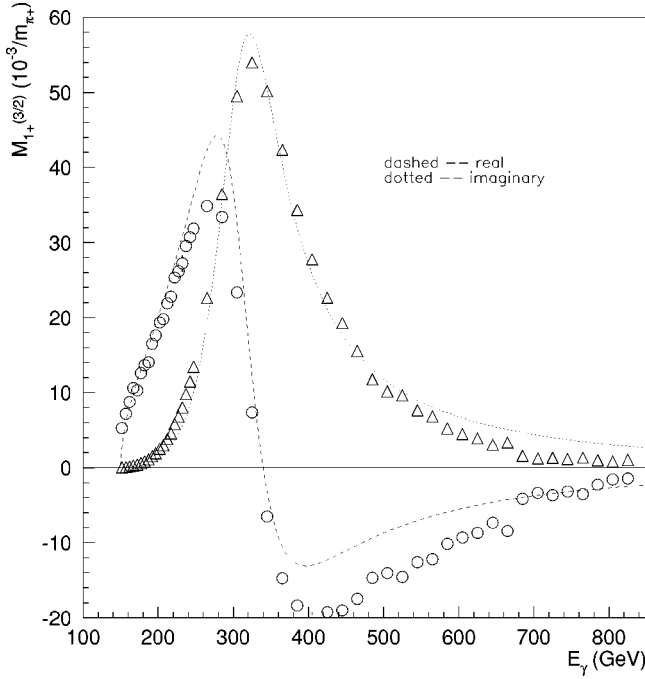


FIG. 2. Real and imaginary parts of the multipole $M_{1+}^{3/2}$ derived from the delta amplitude in π^0 channel. Model results *with* and *without* the quark-model form factor are compared. Data are from SAID analysis (Ref. [27]).

Multipole $E_{1+}^{3/2}$ vanishes in this approach for the s -channel delta resonance. Experimentally, $E_{1+}^{3/2}$ is found to be much smaller than $M_{1+}^{3/2}$ [13,4].

III. RESULTS AND ANALYSIS

In this section, we present our study of reactions, $\gamma p \rightarrow \pi^+ n$, $\gamma p \rightarrow \pi^0 p$, $\gamma n \rightarrow \pi^- p$, and $\gamma n \rightarrow \pi^0 n$ with the same set of coherent parameters. The Goldberger-Treiman relation,

$$g_{\pi NN} = \frac{g_A M_N}{f_\pi}, \quad (42)$$

relates the axial vector coupling g_A to the well-known $g_{\pi NN}$ coupling, where f_π is the pion decay constant. Note that g_A in this model is an overall constant, and can be calculated in the quark model. However, the quark model predicts rather large values: $|g_A| = 5/3$ for charged pions and $5/3\sqrt{2}$ for neutral pions. Consequently, $g_{\pi NN}$ given by Eq. (42) is not a good input for our purpose. On the other hand, $g_{\pi NN}$ is a well-determined number, and we shall therefore “fix” the “parameter” $g_{\pi NN} = 13.48$ in our calculations. This is a strong constraint on the theory, as the Born terms (including seagull term, t -channel pion exchange, and nucleon pole terms) are completely fixed. We shall follow the quark-model predictions for relative signs and strengths in order to study the four charge channels coherently.

A. The charged pion production reaction

A distinguishing feature of π^+ photoproduction is the forward “spike” and the dip near $-t = m_\pi^2$ seen in its differen-

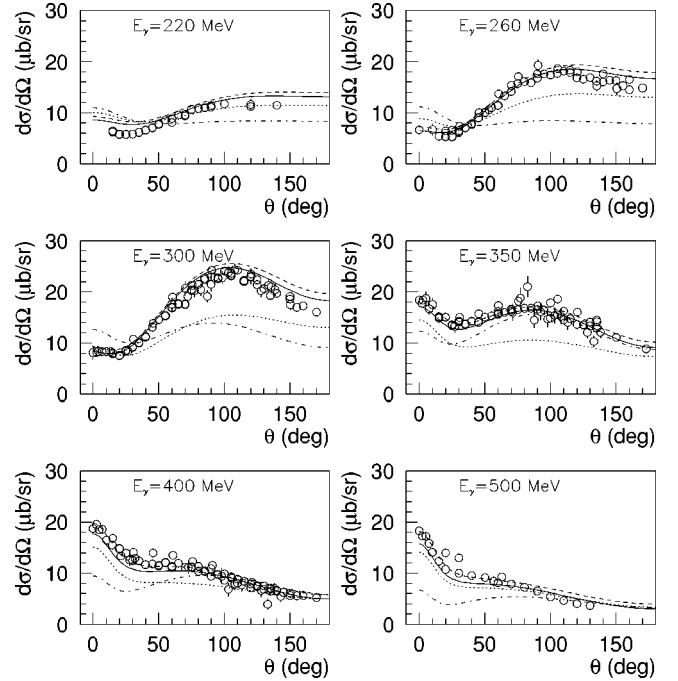


FIG. 3. Differential cross sections for $\gamma p \rightarrow \pi^+ n$. The solid curves denote full calculations with $C_\Delta = 1.7474$; dotted curves, results in the $SU(6) \otimes O(3)$ symmetry limit; dashed curves, results without $n > 1$ u -channel resonance contributions; dot-dashed curves, calculations with resonance, real parts eliminated. Data are from Refs. [28–35].

tial cross sections. Multipole analyses based on a unitary isobaric model and studies utilizing fixed- t dispersion relations suggest that this feature is related to an interference between the Born terms and the delta resonance “excitation” (in the naive quark model, the delta resonance is the ground state for isospin 3/2 baryons). The $M_{1+}^{3/2}$ multipole for the delta resonance dominates the cross sections and single-polarization asymmetries over a wide energy range. Reproducing this combination of features is nontrivial in a microscopic model.

In Fig. 3, we show the calculations for reaction $\gamma p \rightarrow \pi^+ n$ in the $SU(6) \otimes O(3)$ symmetry limit. The dotted curves are calculated in this limit, having only an overall quark-meson coupling parameter, which is in fact not “free” for the Born terms due to the Goldberg-Treiman relation. Near threshold, the cross section is reproduced reasonably, which is consistent with the leading order calculation of chiral perturbation theory. The dip at $-t = m_\pi^2$ clearly originates from the interference between the t -channel pion exchange and the seagull term. At $E_\gamma \leq 220$ MeV, the delta resonance has only small interference.

Interference from the nucleon pole terms becomes important from $E_\gamma = 220$ to 260 MeV. At the lower-energy limit, the t -channel pion exchange and the seagull term dominate over other processes, while for higher energies, the delta resonance dominates. The influence of the nucleon pole terms can be seen clearly in the polarized beam asymmetries. As shown by the dotted curve in Fig. 4 below at $E_\gamma = 260$ MeV, for which the nucleon pole terms are eliminated, the

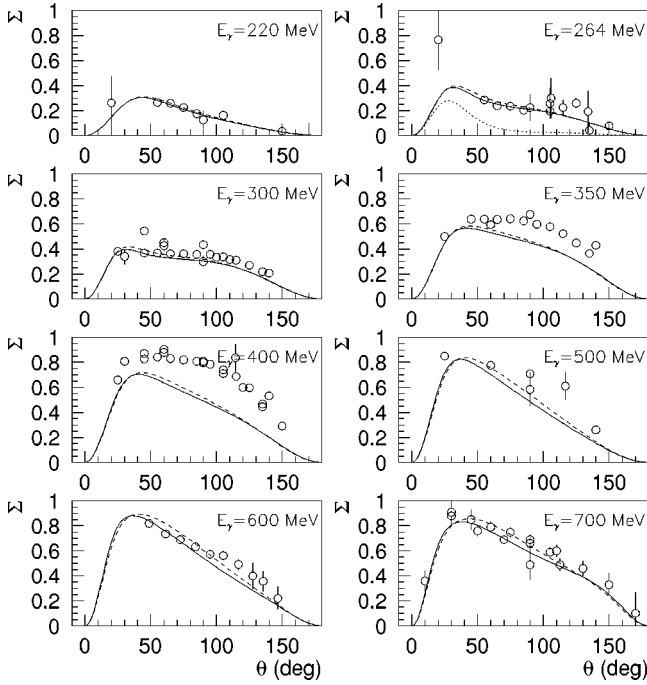


FIG. 4. Polarized beam asymmetry Σ for $\gamma p \rightarrow \pi^+ n$. The solid curves denote full calculations, while the dashed present results without $n > 1$ u -channel resonance contributions. The dotted curve at $E_\gamma = 260$ MeV denotes the effects by eliminating the nucleon pole terms. Data are from Refs. [39–47].

interference from the nucleon pole terms generally produces large asymmetries at intermediate angles.

With increasing energy, we find that the cross sections are underestimated over the delta resonance region in the $SU(6) \otimes O(3)$ symmetry limit. This suggests a failure of the symmetric quark model for the delta resonance. However, notice that the “dip” feature is still sustained over this region, and we assume that the delta excitation has a “good” form factor from the quark model. Thus, we empirically treat the $\pi N \Delta$ coupling strength as a free parameter, which will be fixed by the experimental data. The solid curves shown in Fig. 3 denote the calculations with $C_\Delta = 1.7474$, where $C_\Delta = 1$ is the strength in the quark-model symmetry limit. The enhancement of the delta contribution significantly improves the description of the experimental data. Compared with the dotted curves, the cross sections at the extremely forward and intermediate angles are both enhanced.

The differential cross section for the π^+ production changes rapidly from threshold to the delta resonance region. After that, it remains stable up to $E_\gamma \approx 700$ MeV, where resonances of the second resonance region start to interfere. The challenge for a microscopic approach is not only to reproduce the dramatic changes at low energies, but also to sustain the forward peaking to high energies. It is quite natural for us to achieve the first goal in this model. That is, the enhanced delta resonance succeeds in reproducing the drastic change of the cross sections at the first resonance region. For the second goal, we find that with only one parameter, the strong forward peaking can only be sustained up to $E_\gamma \approx 500$ MeV. This result has nontrivial implications. It sug-

gests that the quark model within an effective Lagrangian provides correct signs and even reasonable form factors for the delta excitation and nucleon pole terms. As illustrated in Sec. II, the delta excitation and the nucleon pole terms have simple structures coming from the harmonic oscillator shell $n = 0$. Clearly, a self-consistent treatment [36] of these ingredients is essential to any viable model. We suggest that the tree level calculation, based on the quark model, may have included the main ingredients (e.g., relative signs and form factors), even though its description of the nucleon pole and delta resonance is very simple.

An interesting question arising in this work is the role played by the u -channel resonance contributions. Generally, this part has been neglected in isobaric models, nor is it included in traditional quark-model calculations, due to empirical considerations [26]. In the present calculation, we find that the u channel process tends to decrease the forward peaking. In Fig. 3, the dashed curves denote calculations with the u channel of $n > 1$ neglected, which enhances the forward peak above the delta resonance region. Since the full calculation underestimates the forward peaking slightly, the neglect of the u channel of $n > 1$ seems to follow the data more closely. This feature seems consistent with findings of Ref. [3]. There, the u -channel resonance contributions were neglected, and an overall strong forward peaking was observed.

Polarization observables are sensitive to resonance contributions, providing a possible way to clarify the role played by the delta resonance. In Fig. 4, the polarized beam asymmetry Σ is calculated for eight energy bins. The results are generally in agreement with the data at $E_\gamma \leq 300$ MeV. However, some discrepancies are found at $E_\gamma = 350$ and 400 MeV, which are sensitive to the u -channel nucleon pole rather than the u -channel resonances ($n > 1$). As shown by the dashed curves, neglecting the $n > 1$ u -channel resonance does not change the solid curves significantly. At $E_\gamma \approx 700$ MeV, the $S_{11}(1535)$ becomes a strongly interfering source. The enhancement of this asymmetry at $\theta = 130^\circ - 140^\circ$ is evidence for the existence of the $S_{11}(1535)$ resonance.

The presence of the $S_{11}(1535)$ as a state of representation [70, 28] in the quark model accounts for Σ naturally up to 750 MeV. Compared with the precise measurement of GRAAL [44], we cannot produce the structure observed at backward angles above 800 MeV. As suggested by the isobaric approach [3], a small $S_{11}(1650)$ contribution can reproduce the data reasonably. In our model calculation, the $S_{11}(1650)$ is absent in the proton reaction due to the Moorhouse selection rule [37]. The breaking of the symmetric quark model will introduce mixing between states of different representations, e.g., the $S_{11}(1535)$ and $S_{11}(1650)$. A more realistic model taking into account such a mixing mechanism is clearly required above the second resonance region. The $S_{11}(1650)$ has large branching fraction to πN states [38].

Calculations for the polarized target asymmetries are presented in Fig. 5, and compared with existing experimental measurements. Given that only one parameter has been introduced, the results should be regarded as consistent with the data from threshold to $E_\gamma \approx 500$ MeV. At E_γ

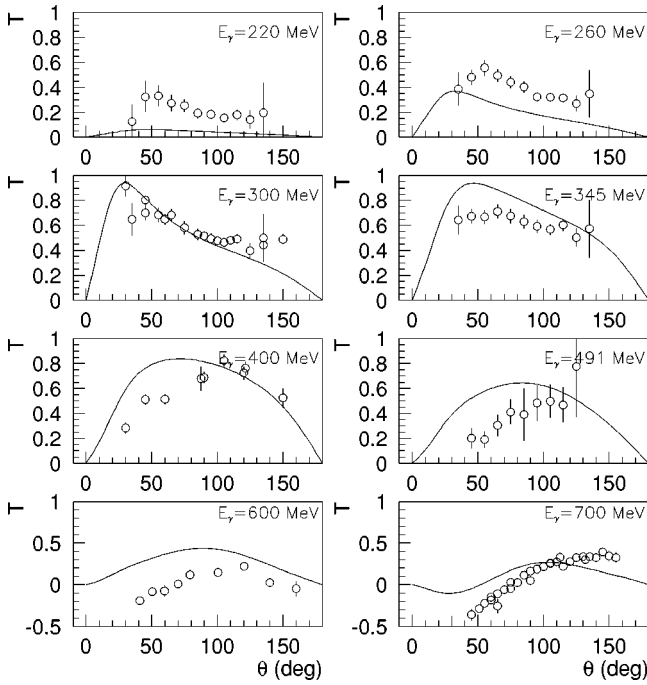


FIG. 5. Polarized target asymmetry T for $\gamma p \rightarrow \pi^+ n$. Data are from Refs. [48,41,49–51].

≈ 220 MeV, our results underestimate the data, however this feature is consistent with the SAID fit [13].

Calculations for the recoil polarization asymmetries are presented in Fig. 6, which are consistent with the data in the first resonance region.

The reaction $\gamma n \rightarrow \pi^- p$ is calculated using the same set of parameters determined in the π^+ production. We present the results for the differential cross sections in Fig. 7. Although large uncertainties exist within the data, our calculation is in good agreement with experiment up to $E_\gamma \approx 400$ MeV. Interestingly, these results, which can be regarded as predictions of this approach, are very close to the analyses of Ref. [4]. It is worth noting that similar structures as found in $\gamma p \rightarrow \pi^+ n$ (the “dip” and “spike”) are also present here, and are due to the same mechanism.

B. The neutral-pion production reaction

In comparison with the charged pion production, the neutral-pion channels are relatively simple in this model. The

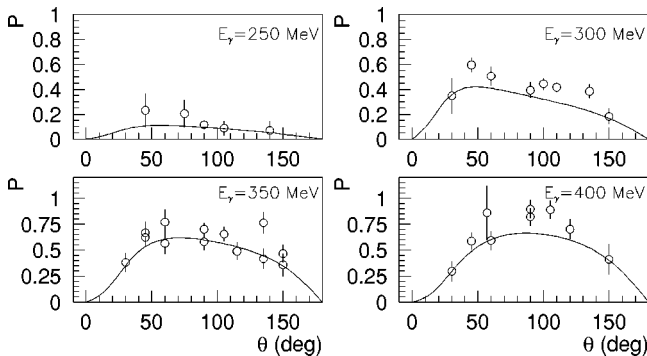


FIG. 6. Recoil polarization asymmetry P for $\gamma p \rightarrow \pi^+ n$. Data are from Refs. [41,52].

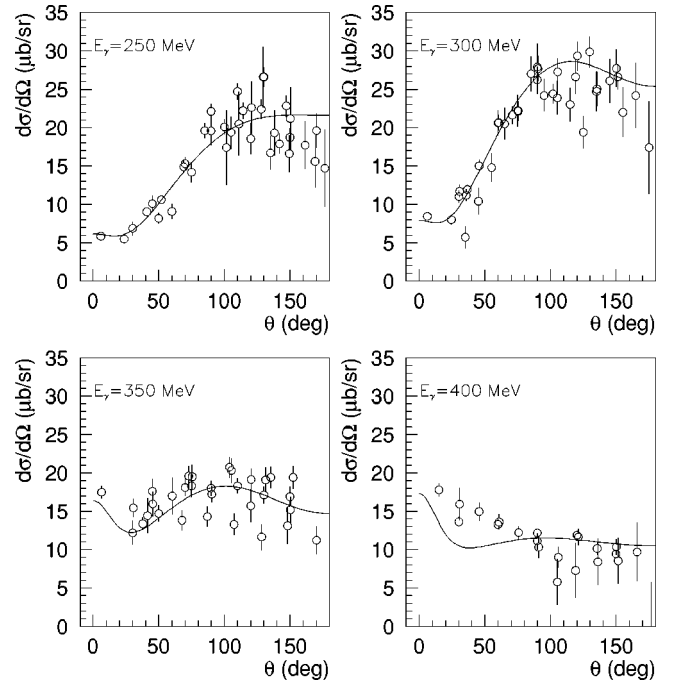


FIG. 7. Differential cross sections for $\gamma n \rightarrow \pi^- p$. Data are from Refs. [33,53–59].

contact term and the t -channel pion exchange are eliminated in the effective interaction since these amplitudes are proportional to the charge of the produced meson. The nucleon pole terms and the delta excitation therefore dominate over other processes near threshold.

In Fig. 8, the differential cross sections for $\gamma p \rightarrow \pi^0 p$ are presented at several energies. In the $SU(6) \otimes O(3)$ symmetry

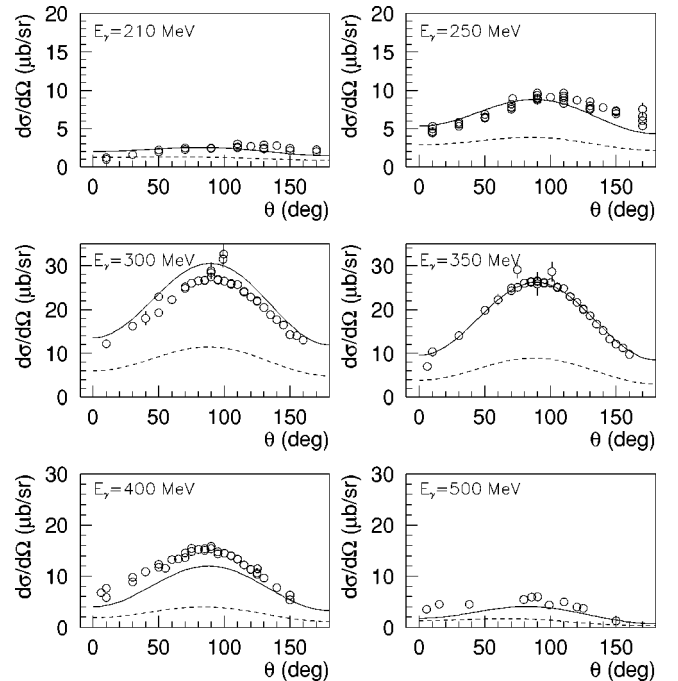


FIG. 8. Differential cross sections for $\gamma p \rightarrow \pi^0 p$. Data are from Refs. [60–68].

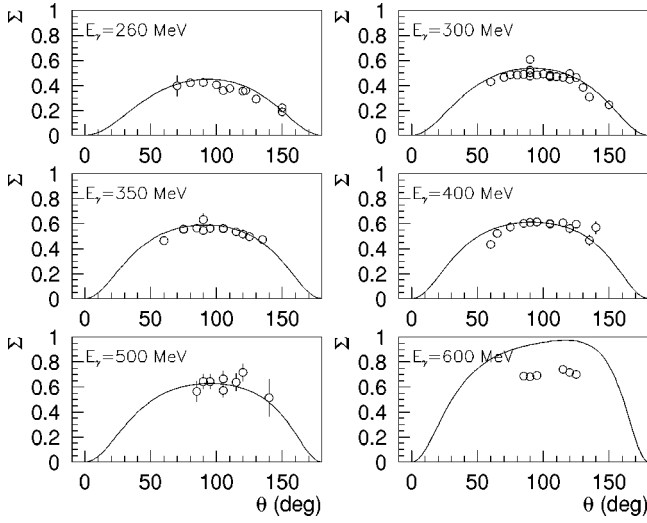


FIG. 9. Polarized beam asymmetry Σ for $\gamma p \rightarrow \pi^0 p$. Data are from Refs. [39,69,62,70–74].

limit, as shown by the dashed curves, the cross sections are underestimated by the delta excitation. Similar to the feature arising from the charged pion production channels, we need to enhance the delta excitation strength to reproduce the data.

The calculations of the single-polarization asymmetries are presented in Figs. 9–11 and compared with data.

In Fig. 12, the calculated cross sections for $\gamma n \rightarrow \pi^0 n$ are presented. So far, there are only sparse data available for this channel.

The above results for the cross section and single-polarization asymmetries suggest an overall quantitative agreement with the data from threshold to the first resonance

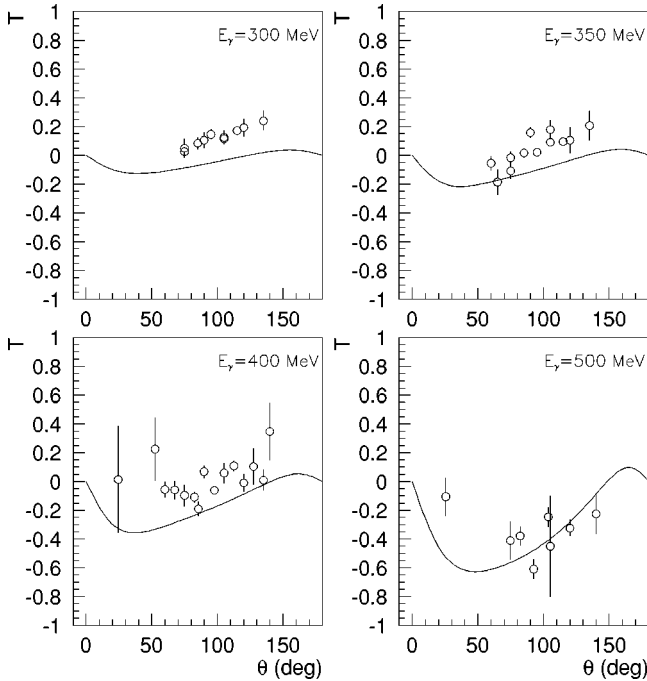


FIG. 10. Polarized target asymmetry T for $\gamma p \rightarrow \pi^0 p$. Data are from Refs. [70,75–77,74].

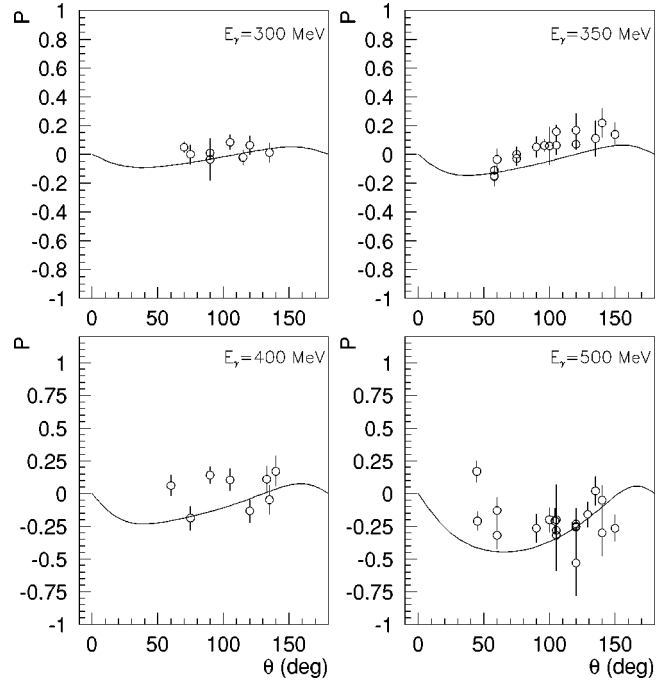


FIG. 11. Recoil polarization asymmetry P for $\gamma p \rightarrow \pi^0 p$. Data are from Refs. [78,70,72,74].

region, while qualitatively, the data up to the second resonance region can be explained. The lack of quantitative agreement above the delta resonance region was expected, given that only a minimum number of free parameters are used here. However, by using only a minimal model, it has been easier to identify key ingredients responsible for those trends we *do* reproduce.

C. Quark-model form factor and the helicity basis

As mentioned previously, in π^+ photoproduction, the most prominent features seen in the cross section are forward peaking and the dip at $-t = m_\pi^2$, which is attributed to the Born terms. Our results also reproduce this feature. Some new ingredients appearing in this approach concern the roles played by the Born terms and the delta resonance, and the influence of their associated form factors.

As found in previous studies, the Born terms deviate significantly from the experimental data at intermediate and

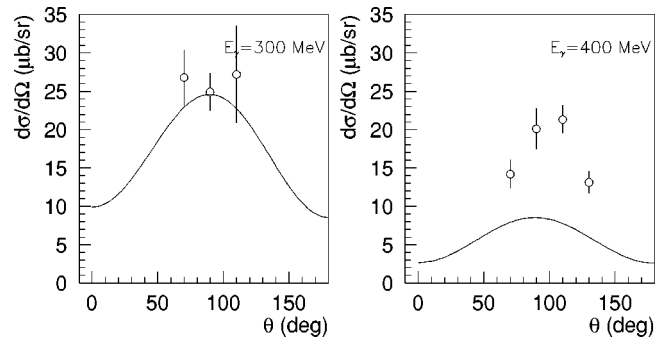


FIG. 12. Differential cross sections for $\gamma n \rightarrow \pi^0 n$. Data are from Ref. [80].

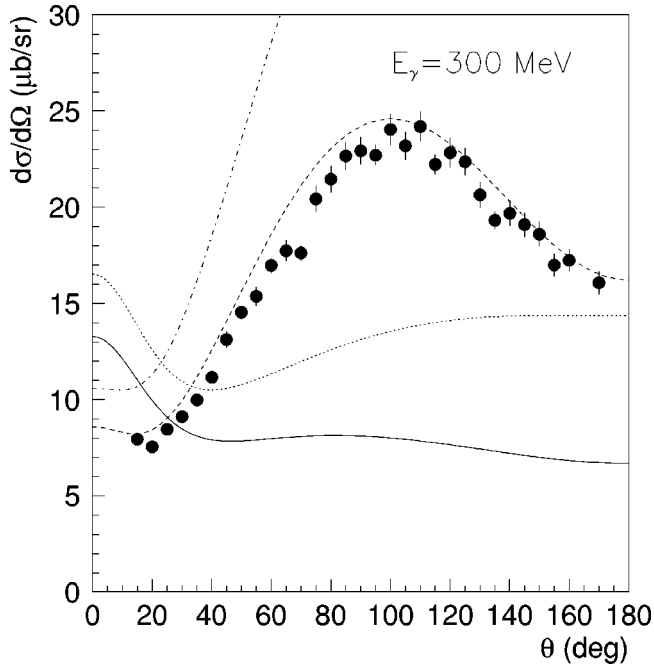


FIG. 13. Cross sections for $\gamma p \rightarrow \pi^+ n$ at 300 MeV. Plotted are the Born terms with (solid curve) and without (dotted) form factor, and the Born terms plus the delta transition with (dashed) and without (dot-dashed) form factors, respectively.

backward angles as photon energies increase to the GeV level. The cross section due to Born terms alone is much larger than the data suggest. One possible explanation is that the Born terms are canceled by resonance contributions away from the forward peak. As discussed by Barbour, Malone, and Moorhouse in a fixed- t dispersion relation [26], the real parts of the resonance amplitudes tend to cancel the Born terms at $-t > m_\pi^2$, while the region $-t < m_\pi^2$ is slightly enhanced by low-lying resonance contributions.

In Fig. 13, we illustrate the results for the Born terms and Born terms plus delta excitation, with and without the quark-j model form factors, respectively. Clearly, form factors are vital in the quark-model description, though no free parameters have been introduced. Comparing the full result to one in which the form factors are switched off, we see potential problems for those who compare quark-model results directly to fits (such as SAID and MAID) which do not introduce form factors. An interesting extension of this work would be the consideration of forward cross sections at higher energies, where the influence of form factors is nebulous [81,36].

To end this section, we present a comparison of energy evolution of the Born terms plus delta helicity amplitudes calculated by this model with a SAID analysis [82]. The four independent helicity amplitudes are calculated following the convention of Ref. [2],

$$\frac{d\sigma}{d\Omega_{c.m.}} = \frac{1}{2} \frac{|\mathbf{q}|}{|\mathbf{k}|} \sum_{i=1}^4 |H_i(\theta_{c.m.})|^2, \quad (43)$$

where $\theta_{c.m.}$ is the angle between the incoming photon mo-

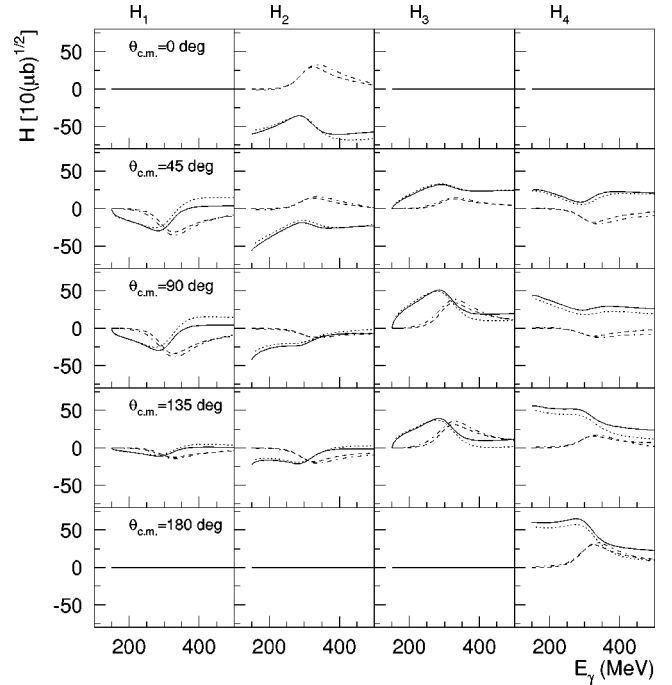


FIG. 14. Energy evolution of the Born terms plus delta helicity amplitudes compared with the SAID analyses. Columns from left to right are amplitudes $H_{1,2,3,4}$. The solid and dashed curves denote the real and imaginary parts calculated by this model, while the dotted and dot-dashed denote those by SAID analyses.

mentum \mathbf{k} and outgoing meson momentum \mathbf{q} in the c.m. system. In Fig. 14, the helicity amplitudes are presented at five angles, $\theta_{cm} = 0^\circ, 45^\circ, 90^\circ, 135^\circ,$ and 180° . At $\theta_{c.m.} = 0^\circ$, only H_2 has nonzero values, while all the other elements vanish. In the backward direction, the nonvanishing element is H_4 . Compared with the SAID analysis, an overall agreement is obtained up to 500 MeV.

D. t -channel vector-meson exchange

A long-standing question concerns the role played by vector-meson exchange in low-energy pion photoproduction. According to the duality argument [83], the introduction of vector-meson exchanges, along with a complete set of s -channel resonances, might result in double counting. In practice, a systematic inclusion of all s -channel resonances at the hadronic level is not available. Empirically, t -channel vector-meson exchange may account for incomplete s -channel resonance contributions, which, however, makes the duality hypothesis more ambiguous.

Given the results presented in the previous subsections, the quark-model framework, with an effective Lagrangian, could address this question in pion photoproduction from a more fundamental level. As seen in the cross sections for π^+ production up to 700 MeV, forward peaking above the delta resonance has been successfully sustained up to 500 MeV. This could reasonably illustrate that the effective Lagrangian has been sufficient to describe the data over the first reso-

nance region. In order to consider the effect of possible double counting between the t -channel vector-meson exchange and s - and u -channel resonances, we compare models including various subsets of these diagrams. Our purpose is to clarify whether the behavior of those higher excited states (terms) would be similar to the inclusion of vector-meson exchange, particularly to compare with an ‘‘isobaric’’ model, where the u -channel resonance contributions are neglected.

We shall introduce the following effective Lagrangians for vector-meson exchange:

$$\mathcal{L}_{\gamma\pi V} = e \frac{g_{\gamma\pi V}}{m_\pi} \varepsilon_{\alpha\beta\gamma\delta} \partial^\alpha A^\beta \partial^\gamma V^\delta \pi, \quad (44)$$

for $\gamma\pi V$ coupling and

$$\mathcal{L}_{Vqq} = g_{Vqq} \bar{\psi} \left(\gamma_\mu + \frac{\kappa_q}{2m_q} \sigma_{\mu\nu} \partial^\nu \right) V^\mu \psi, \quad (45)$$

for the quark-vector-meson (V - qq) coupling; A and V denote the photon and vector meson; π denotes the pion field; ψ ($\bar{\psi}$) denotes the quark (antiquark) field; $g_{\gamma\pi V}$ and g_{Vqq} are coupling constants. Note that we treat the V - qq coupling at quark level in order to be consistent with our framework. In this way, there is once again no need to introduce free parameters for the vertex form factors. In addition, a simple current analogy will relate the g_{Vqq} to g_{VNN} , constraining this term as well.

Some simple algebra gives the transition amplitude,

$$\begin{aligned} \mathcal{M}_V = & e \frac{g_{V\pi\gamma} g_{Vqq} e^{-(\mathbf{k}-\mathbf{q})^2/6\alpha^2}}{m_\pi(t-m_\pi^2)} \left\{ g_t \left[1 + \frac{\omega_m}{E_f+M_f} + \frac{\omega_\gamma}{E_i+M_i} + \frac{\kappa_q}{2m_q} \left\{ \frac{m_\pi^2}{E_f+M_f} - \left(\frac{1}{E_f+M_f} + \frac{1}{E_i+M_i} k \cdot q \right) \right\} \right] \mathbf{q} \cdot (\mathbf{k} \times \boldsymbol{\epsilon}_\gamma) \right. \\ & + g_A \left[\frac{\omega_\gamma \mathbf{q}^2}{E_f+M_f} + \frac{\omega_m \mathbf{k}^2}{E_i+M_i} - \left(\frac{\omega_\gamma}{E_i+M_i} + \frac{\omega_m}{E_f+M_f} \right) \mathbf{q} \cdot \mathbf{k} + \frac{\kappa_q}{2m_q} \left\{ \omega_m \mathbf{k}^2 + \omega_\gamma \mathbf{q}^2 + \frac{\omega_\gamma \omega_m}{E_f+M_f} \mathbf{q}^2 \right. \right. \\ & + \left. \left. \frac{(\omega_\gamma \omega_m - m_\pi^2)}{E_i+M_i} \mathbf{k}^2 - \left(\omega_\gamma + \omega_m + \frac{\omega_m^2}{E_f+M_f} + \frac{\omega_\gamma^2}{E_i+M_i} - \frac{k \cdot q}{E_i+M_i} + \frac{\mathbf{q} \cdot \mathbf{k}}{E_f+M_f} \right) \mathbf{q} \cdot \mathbf{k} \right\} \right] i \boldsymbol{\sigma} \cdot \boldsymbol{\epsilon}_\gamma \\ & + g_A \left[\frac{\omega_m}{E_f+M_f} + \frac{\kappa_q}{2m_q} \left(\omega_m + \frac{\omega_m^2}{E_f+M_f} - \frac{k \cdot q}{E_f+M_f} + \frac{\mathbf{k} \cdot \mathbf{q}}{E_i+M_i} \right) \right] i \boldsymbol{\sigma} \cdot \mathbf{k} \mathbf{q} \cdot \boldsymbol{\epsilon}_\gamma \\ & \left. - g_A \left[\frac{\omega_\gamma}{E_f+M_f} + \frac{\kappa_q}{2m_q} \left(\omega_\gamma + \frac{\mathbf{k}^2}{E_i+M_i} + \frac{\omega_\gamma \omega_m}{E_f+M_f} \right) \right] i \boldsymbol{\sigma} \cdot \mathbf{q} \mathbf{q} \cdot \boldsymbol{\epsilon}_\gamma \right\}, \quad (46) \end{aligned}$$

where $k \cdot q = \omega_\gamma \omega_m - \mathbf{k} \cdot \mathbf{q}$ is the four-momentum product; the exponent comes from the nucleon wave functions, which plays the role of a form factor; g_A is the axial vector coupling and defined in the quark model as Eq. (16), i.e.,

$$\langle N_f | \sum_j \hat{I}_j^v \boldsymbol{\sigma}_j | N_i \rangle \equiv g_A \langle N_f | \boldsymbol{\sigma} | N_i \rangle, \quad (47)$$

where \hat{I}_j^v is the isospin operator for the exchanged vector meson. The other factor g_t comes from the isospin space,

$$g_t \equiv \langle N_f | \sum_j \hat{I}_j^v | N_i \rangle. \quad (48)$$

Analogy between the quark level operator and V - NN coupling gives

$$g_t g_{Vqq} = g_{VNN},$$

$$g_A \frac{g_{Vqq}}{m_q} (1 + \kappa_q) = \frac{g_{VNN}}{m_N} (1 + \kappa_V), \quad (49)$$

where $m_q = 330$ MeV is the constituent quark mass. In Ref. [84], a similar relation was investigated, but only the vector current was introduced for the V - qq coupling. We shall use the commonly used values for g_{VNN} and κ_V to constrain the values for g_{Vqq} and κ_q .

In the π^+ production, we adopt the values $g_{\rho NN} = 3$ and $\kappa_\rho = 3.71$ as inputs. With the quark-model values $g_A = 5/3$ and $g_t = 1$ for $\gamma p \rightarrow \pi^+ n$, we derive $g_{\rho qq} = 3$ and $\kappa_q^\rho = -0.0064$. In $\gamma p \rightarrow \pi^0 p$, we adopt $g_{\omega NN} = 9$, and $\kappa_\omega = -0.12$. With $g_A^\omega = 1$ and $g_t^\omega = 3$, $g_{\omega qq} = 3$ and $\kappa_q^\omega = 0.2$ are derived for the ω exchange, and with $g_A^\rho = 5/3\sqrt{2}$ and $g_t^\rho = 1/\sqrt{2}$, $g_{\rho qq} = 3$ and $\kappa_q^\rho = -1.99$ are derived.

In Figs. 15 and 16, we show the calculations of observables ($d\sigma/d\Omega$, Σ , T , and P) with the t -channel vector-meson exchange (VME) for $\gamma p \rightarrow \pi^+ n$ and $\gamma p \rightarrow \pi^0 p$, respectively. Three energy bins are investigated. We use $s + u$

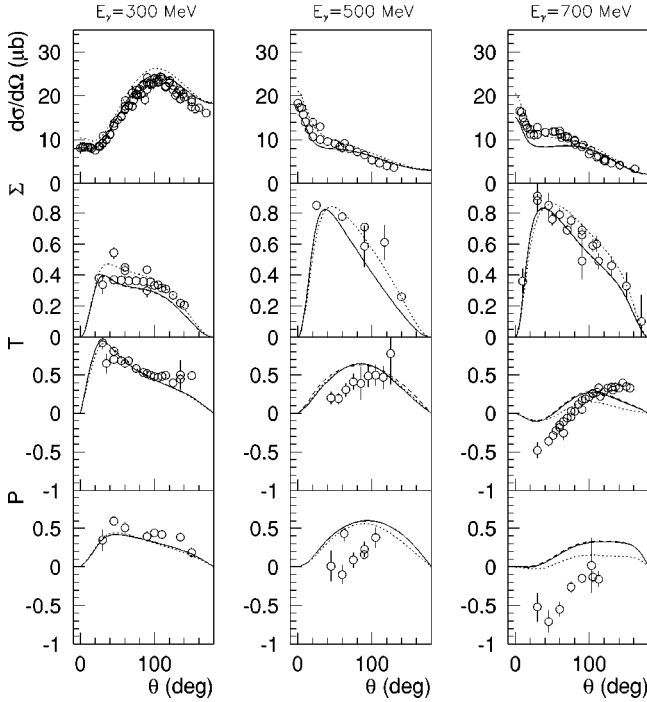


FIG. 15. Observables for $\gamma p \rightarrow \pi^+ n$ at three energies. Solid curves denote results for $s+u$; dashed for $s+u+t$; and dotted for $s+t$. Data are from Refs. [85,86,28,87,45–48,88,89].

to denote the effective Lagrangian calculations, while $s+t$ denotes calculations suppressing the u -channel resonance but including the t -channel VME. Finally, we use $s+u+t$ to represent the full calculation, including the VME. The values, $g_{\rho\pi\gamma}=0.103$ and $g_{\omega\pi\gamma}=0.313$, are adopted.

In the π^+ production, contributions from the VME are found to be negligible. One reason is the relatively smaller couplings of $g_{\rho\pi\gamma}$ and $g_{\rho NN}$ compared to the couplings for ω exchange. However, the main factor leading to small VME contributions in the π^+ production is a large cancellation occurring among terms proportional to g_A and g_t in Eq. (46). Since different contributions from the VME to different reactions depend on the quark-model prediction for g_A and g_t , the VME might introduce more model-dependent ingredients in the calculations.

IV. CONCLUSIONS

We have studied pion photoproduction in four charge channels within the quark model incorporating an effective Lagrangian. Up to $E_\gamma=500$ MeV, the cross sections and single-polarization asymmetries can be accounted for with one adjustable parameter for the delta excitation strength. We find that if a stronger coupling for the delta transition is employed, all the observables in the first resonance region can be reproduced. In other words, the nonrelativistic constituent quark model (NRCQM) might have provided a reasonable form factor for the delta resonance, but with weaker coupling.

As the first systematic microscopic study of pion photoproduction, this result suggests that a direct calculation of the tree level diagrams based on the quark model with a chiral

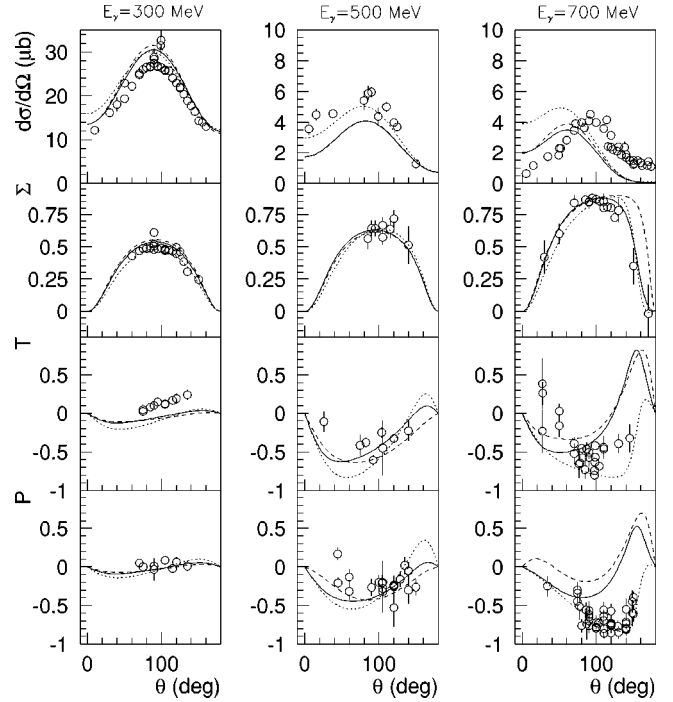


FIG. 16. Observables for $\gamma p \rightarrow \pi^0 p$ at three energies. Solid curves denote results for $s+u$; dashed for $s+u+t$; and dotted for $s+t$. Data are from Refs. [90,67,91,92,68,45,73,93,77,76,94,79].

effective Lagrangian may contain the main ingredients required in an elementary approach. In particular, we show that the quark-model form factors play a key role in reproducing the data over a wide energy region. Such a form factor can be only self-consistently and completely considered in a direct calculation of quark level diagrams. This result highlights the relation between the background Born terms and resonance excitations. Extensions to higher energies would help to clarify the relation between quark-model results and those found via phenomenology. Nevertheless, a parallel investigation of electroproduction would be useful for a better understanding of the delta resonance based on this model. We shall report this elsewhere.

Restricted to the low energies at $E_\gamma < 500$ MeV, we see that t -channel vector-meson exchange is negligible. This leaves the duality hypothesis far from conclusive. We expect that more sophisticated calculations at high energies could be helpful in disentangling this question as well.

ACKNOWLEDGMENTS

Useful discussions with F. E. Close and T. Sato are gratefully acknowledged. Q.Z. thanks J. Arends for sending details about their experimental data. Q.Z. and J.A. acknowledge the financial support of the United Kingdom Engineering and Physical Sciences Research Council (Grant No. GR/M82141). R.W. acknowledges the financial support in part by U.S. Department of Energy (DOE) Grant No. DE-FG02-99ER41110. R.W. also acknowledges partial support from Jefferson Lab, by the Southeastern Universities Research Association under DOE Contract No. DE-AC05-84ER40150.

- [1] S. Capstick and W. Roberts, *Prog. Part. Nucl. Phys.* **45**, 5241 (2000).
- [2] R.L. Walker, *Phys. Rev.* **182**, 1729 (1969).
- [3] D. Drechsel, O. Hanstein, S.S. Kamalov, and L. Tiator, *Nucl. Phys.* **A645**, 145 (1999).
- [4] O. Hanstein, D. Drechsel, and L. Tiator, *Nucl. Phys.* **A632**, 561 (1998).
- [5] I.G. Aznauryan and S.G. Stepanyan, *Phys. Rev. D* **59**, 054009 (1999).
- [6] R.L. Crawford, talk given at Workshop on the Physics of Excited Nucleons, Mainz, Germany, 2001 (NSSTAR 2001), p. 163.
- [7] R.M. Davidson, N.C. Mukhopadhyay, and R.S. Wittman, *Phys. Rev. D* **43**, 71 (1991).
- [8] S. Nozawa, B. Blankleider, and T.-S.H. Lee, *Nucl. Phys.* **A513**, 459 (1990).
- [9] S. Nozawa and T.-S.H. Lee, *Nucl. Phys.* **A513**, 511 (1990).
- [10] H. Garcilazo and E. Moya de Guerra, *Nucl. Phys.* **A562**, 521 (1993).
- [11] T. Sato and T.-S.H. Lee, *Phys. Rev. C* **54**, 2660 (1996); **63**, 055201 (2001).
- [12] Z. Li, R.A. Arndt, L.D. Roper, and R.L. Workman, *Phys. Rev. C* **47**, 2759 (1993).
- [13] R.A. Arndt, I.I. Strakovsky, and R.L. Workman, *Phys. Rev. C* **53**, 430 (1996).
- [14] Z.-P. Li, H.-X. Ye, and M.-H. Lu, *Phys. Rev. C* **56**, 1099 (1997).
- [15] Z.-P. Li, *Phys. Rev. D* **52**, 4961 (1995).
- [16] Z.-P. Li and B. Saghai, *Nucl. Phys.* **A644**, 345 (1998).
- [17] Q. Zhao, B. Saghai, and Z.-P. Li, *J. Phys. G* **28**, 1293 (2002).
- [18] B. Saghai and Z.-P. Li, *Eur. Phys. J. A* **11**, 217 (2001).
- [19] Z.-P. Li, *Phys. Rev. C* **52**, 1648 (1995).
- [20] Z.-P. Li, W.H. Ma, and L. Zhang, *Phys. Rev. C* **54**, 2171 (1996).
- [21] Z.-P. Li, *Phys. Rev. D* **50**, 5639 (1994).
- [22] Le Yaouance *et al.*, *Hadron Transitions in the Quark Model* (Gordon and Breach, New York, 1988).
- [23] Z.-P. Li, *Phys. Rev. D* **48**, 3070 (1993).
- [24] G.F. Chew, M.L. Goldberger, F.E. Low, and Y. Nambu, *Phys. Rev.* **106**, 1345 (1957).
- [25] C.G. Fasano, F. Tabakin, and B. Saghai, *Phys. Rev. C* **46**, 2430 (1992).
- [26] I. Barbour, W. Malone, and R.G. Moorhouse, *Phys. Rev. D* **4**, 1521 (1971).
- [27] SAID online database, <http://gwdac.phys.gwu.edu>
- [28] K. Buechler *et al.*, *Nucl. Phys.* **A570**, 580 (1994).
- [29] G. Fischer *et al.*, *Nucl. Phys.* **B16**, 119 (1970).
- [30] G. Fischer *et al.*, *Z. Phys.* **253**, 38 (1972).
- [31] E.A. Knapp *et al.*, *Phys. Rev.* **114**, 605 (1963).
- [32] C. Betourne *et al.*, *Phys. Rev.* **172**, 1343 (1968).
- [33] Y. Fujii *et al.*, *Nucl. Phys.* **B120**, 395 (1977).
- [34] D. Branford *et al.*, *Phys. Rev. C* **61**, 014603 (2000).
- [35] K.H. Althoff *et al.*, *Z. Phys. C* **18**, 199 (1983).
- [36] R.L. Workman, talk given at Workshop on the Physics of Excited Nucleons, Mainz, Germany, 2001 (NSSTAR, 2001), p. 101.
- [37] R.G. Moorhouse, *Phys. Rev. Lett.* **16**, 772 (1966).
- [38] Particle Data Group, D. E. Groom *et al.*, *Eur. Phys. J. C* **15**, 1 (2000).
- [39] G. Blanpied *et al.*, *Phys. Rev. C* **64**, 025203 (2001).
- [40] V.N. Zabaev *et al.*, *Yad. Fiz.* **21**, 551 (1975) [*Sov. J. Nucl. Phys.* **21**, 286 (1975)].
- [41] V.A. Getman *et al.*, *Nucl. Phys.* **B188**, 397 (1981).
- [42] V.B. Ganenko *et al.*, *Yad. Fiz.* **23**, 100 (1976) [*Sov. J. Nucl. Phys.* **23**, 52 (1976)].
- [43] F.F. Liu *et al.*, *Phys. Rev.* **144**, 1093 (1966).
- [44] J. Ajaka *et al.*, *Phys. Lett. B* **475**, 372 (2000).
- [45] G. Knies *et al.*, *Phys. Rev. D* **10**, 2778 (1974).
- [46] P.J. Bussey *et al.*, *Nucl. Phys.* **B154**, 205 (1979).
- [47] J. Alspector *et al.*, *Phys. Rev. Lett.* **28**, 1403 (1972).
- [48] H. Dutz *et al.*, *Nucl. Phys.* **A601**, 319 (1996).
- [49] S. Arai *et al.*, *Nucl. Phys.* **B48**, 397 (1972).
- [50] T. Fukushima *et al.*, *Nucl. Phys.* **B130**, 486 (1977).
- [51] K.H. Althoff *et al.*, *Phys. Lett.* **59B**, 93 (1975).
- [52] K.H. Althoff *et al.*, *Phys. Lett.* **26B**, 640 (1968).
- [53] A. Bagheri *et al.*, *Phys. Rev. C* **38**, 875 (1988).
- [54] A.M. Rossi *et al.*, *Nuovo Cimento A* **13**, 59 (1973).
- [55] M.T. Tran *et al.*, *Nucl. Phys.* **A324**, 301 (1978).
- [56] P. Argan *et al.*, *Nucl. Phys.* **A296**, 373 (1978).
- [57] P.A. Berardo *et al.*, *Phys. Rev. D* **9**, 621 (1974).
- [58] P. Benz *et al.*, *Nucl. Phys.* **B65**, 158 (1973).
- [59] G. Von Holtey *et al.*, *Nucl. Phys.* **B70**, 379 (1974).
- [60] C. Fuchs *et al.*, *Phys. Lett. B* **368**, 20 (1996).
- [61] H. Genzel *et al.*, *Z. Phys.* **268**, 43 (1974).
- [62] R. Beck *et al.*, *Phys. Rev. Lett.* **78**, 606 (1997).
- [63] B.M. Aleksandrov *et al.*, *Sov. J. Nucl. Phys.* **28**, 344 (1978).
- [64] Y. Hemmi *et al.*, *Phys. Lett.* **43B**, 79 (1973).
- [65] P. Dougan *et al.*, *Z. Phys. A* **280**, 341 (1977).
- [66] P. Argan *et al.*, *Nucl. Phys.* **A237**, 447 (1975).
- [67] M. Yoshioka *et al.*, *Nucl. Phys.* **B168**, 222 (1980).
- [68] Y. Hemmi *et al.*, *Nucl. Phys.* **B55**, 333 (1973).
- [69] G. Blanpied *et al.*, *Phys. Rev. Lett.* **69**, 1880 (1992).
- [70] V.B. Belyaev *et al.*, *Nucl. Phys.* **B213**, 201 (1983).
- [71] G. Barbiellini *et al.*, *Phys. Rev.* **184**, 1402 (1969).
- [72] V.G. Gorbenko *et al.*, *Yad. Fiz.* **27**, 1204 (1978) [*Sov. J. Nucl. Phys.* **27**, 638 (1978)].
- [73] G.G. Adamian *et al.*, *Phys. Rev. C* **63**, 054606 (2001).
- [74] V.G. Gorbenko *et al.*, *Yad. Fiz.* **26**, 320 (1977) [*Sov. J. Nucl. Phys.* **26**, 167 (1977)].
- [75] M.M. Block *et al.*, *Phys. Rev. Lett.* **81**, 534 (1998).
- [76] M. Fukushima *et al.*, *Nucl. Phys.* **B136**, 189 (1978).
- [77] P. Feller *et al.*, *Nucl. Phys.* **B110**, 397 (1976).
- [78] K.H. Althoff *et al.*, *Phys. Lett.* **26B**, 677 (1968).
- [79] K. Kato *et al.*, *Nucl. Phys.* **B168**, 1 (1980).
- [80] A. Ando *et al.*, *Physik Daten*, 1977 (unpublished).
- [81] R.M. Davidson and R.L. Workman, *Phys. Rev. C* **63**, 058201 (2001).
- [82] Plotted is a SAID analysis containing the unitarized Born terms plus Delta multipoles found in a fit to data (up to 2 GeV).
- [83] R. Dolen, D. Horn, and C. Schmid, *Phys. Rev.* **166**, 1768 (1966); R. Williams, C.R. Ji, and S. Cotanch, *Phys. Rev. C* **43**, 452 (1991); **46**, 1617 (1992).
- [84] D.O. Riska and G.E. Brown, *Nucl. Phys.* **A679**, 577 (2001).
- [85] Y. Fujii *et al.*, *Phys. Rev. Lett.* **26**, 1672 (1971).
- [86] H.W. Dannhausen *et al.*, *Eur. Phys. J. A* **11**, 441 (2001).
- [87] S.D. Ecklund *et al.*, *Phys. Rev.* **159**, 1195 (1967).
- [88] K.H. Althoff *et al.*, *Phys. Lett.* **63B**, 107 (1976).

- [89] K. Egawa *et al.*, Nucl. Phys. **B188**, 11 (1981).
[90] B. Krusche *et al.*, Eur. Phys. J. A **6**, 309 (1999).
[91] P. Dougan *et al.*, Z. Phys. A **274**, 73 (1975).
[92] K.H. Althoff *et al.*, Z. Phys. C **1**, 327 (1979).
[93] P.S.L. Booth *et al.*, Nucl. Phys. **B121**, 45 (1977).
[94] A.A. Zyalov *et al.*, Yad. Fiz. **28**, 105 (1978) [Sov. J. Nucl. Phys. **28**, 52 (1978)].